Electrosynthesized CuMgAl Layered Double Hydroxides as New Catalysts for the Electrochemical Reduction of CO2

Electrosynthesized CuMgAl Layered Double Hydroxides as New Catalysts for the Electrochemical Reduction of CO_2

Martina Serafini, Federica Mariani, Andrea Fasolini, Eleonora Tosi Brandi, Erika Scavetta, Francesco Basile, and Domenica Tonelli**

M. Serafini, F. Mariani, A. Fasolini, E. Tosi Brandi, E. Scavetta, F. Basile, D. Tonelli
Department of Industrial Chemistry "Toso Montanari"
University of Bologna
Viale del Risorgimento, 4, 40136 Bologna, Italy
*Corresponding Authors
E-mail:
f.basile@unibo.it, orcid.org/0000-0003-1379-6418 (F. Basile)
domenica.tonelli@unibo.it, orcid.org/0000-0002-2844-9817 (D. Tonelli)

Keywords: CuMgAl layered double hydroxides, Cu species, composite materials, acetic acid, CO_2 electrochemical conversion, Gas Diffusion Layers

ABSTRACT

In this work, new nanostructured CuMgAl Layered Double Hydroxide (LDH) based materials have been synthesized on a 4 cm^2 sized carbonaceous gas diffusion membrane. By means of microscopic and spectroscopic techniques, the catalysts have been thoroughly investigated, revealing the presence of several species within the same material. By a one-step, reproducible potentiodynamic deposition it is possible to obtain a composite catalyst with an intimate contact between a ternary CuMgAl LDH and Cu^0/Cu_2O species. The catalysts compositions have been investigated by varying: the molar ratio between the total amount of bivalent cations and Al^{3+}, the amount of loaded catalyst, and the molar ratios among the three cations in the electrolytic baths. Each electrocatalyst feature has been evaluated based on the catalytic performances toward the electrochemical CO_2 reduction to acetic acid at -0.4 V vs RHE in a liquid phase configuration. The optimized catalyst, i.e., CuMgAl 2:1:1 LDH exhibits a productivity of 2.0 $mmol_{CH3COOH}\ g_{cat}^{-1}\ h^{-1}$. This result shows the beneficial effects of combining a material like the LDHs, alkaline in nature, and thus with a great affinity to CO_2,

with Cu^0/Cu^+ species, which couples the increase of carbon sources availability at the electrode with a redox mediator capable to convert CO_2 into a C_2 product.

1. Introduction

Carbon dioxide is the second most abundant greenhouse gas in the atmosphere, after water vapor.[1] In the last 200 years average CO_2 levels have increased from 280 to 420 ppm and keep growing despite the mitigation policies introduced in many industrialized countries.[2,3] Nowadays, most of the industrial processes still demand the extensive use of fossil fuels, thus making it unlikely to become independent from these energy resources immediately and completely. However, the need to mitigate the carbon dioxide emissions, and thus to reduce its concentration in the atmosphere, is urgent.[4] Due to the scarce efficacy of the strategies pursued so far for limiting CO_2 emissions alone, the idea of using CO_2 as a possible feedstock is becoming a concrete opportunity.[5] Indeed, several products can be obtained from carbon dioxide, subdivided in long-lived products such as cement, durable polymers, or building insulators, and short-lived products which include fuels and chemicals. Although the long-lived products are capable to reduce CO_2 emissions over a long run, the possibility to develop new platforms capable to enhance the conversion toward fuels and chemicals is attracting growing scientific interest. Among these compounds, C_2 products represent the main building blocks for many chemical syntheses and they have the highest industrial values.[6] For these reasons, much effort has been invested to obtain such commodities from the direct hydrogenation of the CO_2 at ambient operative conditions employing non-critical raw materials, paving the way to the development of a circular economy in which decarbonization route takes place through a "green carbon recycling".[3,7] The conversion of the carbon dioxide can be achieved through different approaches, which involve biochemical,[8,9] radiochemical,[10] thermochemical,[11–13] photochemical,[14,15] or electrochemical reactions.[16,17] Among these, the electrocatalytic reduction is particularly attractive by virtue

of its mild operative conditions, its easily customized reaction outcomes, and its great potential toward scale up.[18–20]

In addition, the electrons required for the activation of the CO_2 molecule can be directly gained from renewable sources, ensuring an eco-friendly alternative and setting the scene toward the fascinating concept of the solar light-driven chemistry.[17,21–23] However, to seize all the benefits that the electrochemical approach can provide and to make it affordable from an industrial point of view,[24] the design of the electrocatalyst plays a key role. To date, strong push has been given to the utilization of sustainable materials, which find their best candidates in the carbon-based electrodes.[19,25] Thanks to their earth abundance, low-cost, great potential window, and reasonably inert electrochemical nature, such materials have been widely employed in the electrocatalysis field.[26–28] Among them, due to the gaseous nature of the carbon dioxide and its mass transport limitations especially in aqueous electrolytes, carbonaceous large-area gas diffusion membranes (GDEs) represent a promising alternative to the classical bulk metal catalysts in order to provide higher current densities, locally generating a gas-solid-liquid microenvironment and maintaining the advantages of being lightweight and low-cost.[29,30] However, the carbonaceous material itself has a negligible catalytic activity toward the CO_2 electroreduction, as neutral carbon atoms can hardly activate the CO_2 molecule which has a high thermodynamic stability, with a binding energy of the C=O double bond of 750 kJ mol^{-1}. Indeed, to achieve the initial radical $CO_2^{\bullet-}$ a very negative potential is needed (-1.3 V vs Ag/AgCl in water).[27]

For this reason, a modification to improve the electrochemical performances, thus enhancing the catalytic activities and selectivity of the material, is needed. The two most commonly pursued strategies are (i) doping carbon materials with heteroatoms such as nitrogen, boron, or sulphur, which provide functional groups capable to convert CO_2 mainly into CO and HCOOH[31–34] and (ii) adding metal or metal oxides, by means of physical or chemical

processes, which allows to modulate the selectivity and the productivity toward C_1 and $\geq C_2$ products.[25,35]

Among them, Cu has been demonstrated to be the only metal capable of catalyzing the CO_2ER into complex hydrocarbons and alcohols with considerable Faradaic Efficiencies (FE).[36]

What makes Cu unique is the ability to bind the key radical anion ($*CO_2^{\bullet-}$). In particular, starting from the pioneering Hori's studies on the bare Cu foil in the 1985,[37] it was demonstrated that copper-based electrocatalysts are capable of producing low carbon content compounds like CO or HCOOH, but also CH_4 and C_2H_4 in significant amounts.[38] Moreover, more recent works have demonstrated also the importance of catalyst morphology and active redox couples that take part in the reaction. On one hand, micro or nanostructured Cu-based catalysts allow to finely tune the reaction outcomes to the desired compounds, enhancing the reaction selectivity and the Faradaic Efficiency.[16,39–43] On the other hand, although the reaction mechanism is still under debate, many research groups have recently proved that catalysts containing adjacent Cu^0 and Cu^I sites are mainly capable to activate the CO_2 reduction and the C-C coupling.[17,44–47] However, while the production of two electrons-transfer compounds like CO or HCOOH has already reached FE close to 100%,[48] $\geq C_2$ compounds are generally produced at relatively high potentials resulting in prohibitively high efficiency losses and low FE.[49] Interestingly, it has been recently demonstrated the ability of nanostructured Cu-based electrocatalysts (containing Cu^0 and Cu_2O species), loaded on carbonaceous supports, to drive the reaction toward the production of CH_3COOH in liquid phase configuration combining low overpotential with high selectivity.[17,40,50] The production of acetic acid is of particular interest from an industrial point of view due to its wide applicability in many chemical sectors.[51] Up to now, the request of acetic acid is fulfilled by industrial multistep fermentative and chemical processes.[51] Among them, Monsanto and Cativa routes, being the most common processes used for the large-scale production of acetic

acid, involve the use of precious metals such as rhodium or iridium-based catalysts and harsh operative conditions.[52]

Therefore, Cu-based electrocatalysts supported on carbonaceous sustainable materials may outperform the classical industrial approaches reducing the number of process steps by directly converting carbon dioxide and operating in cleaner and milder conditions.[53]

As already discussed, while the use of a 3D carbonaceous support helps to enhance mass transport phenomena and, therefore, current densities, the productivity of these systems still suffers from the low solubility of gaseous CO_2 in aqueous environment at room temperature (~34 mM).[43,54] With the aim to increase the CO_2 availability at the electrode surface and thus improve the performances of the Cu-based GDEs, Perry et al.[55] have reported the implementation of polymers with intrinsic microporosity (PIMs) within copper catalysts, showing increased selectivity and production of C_2H_4 thanks to their porosity that reduces the formation of bubbles at the catalyst surface.[56] Similarly, metal−organic frameworks (MOFs) represent another class of nanomaterials with well-developed porosity that have been widely investigated for CO_2 adsorption and electro-conversion toward methane[57] or > C_1 products.[58] Interestingly, there is another class of compounds that, due to their alkaline nature and high affinity for carbonates, may have a great potential in CO_2ER applications. Also known as hydrotalcites-like compounds, Layered Double Hydroxides (LDHs) are anionic clays with molecular formula $[(M^{II})_{1-x}(M^{III})_x(OH)_2]^{x+}(A^{n-}_{x/n}) \cdot mH_2O$, coming from the natural hydrotalcite $Mg_6Al_2(OH)_{16}(CO_3) \cdot 4H_2O$. They consist of lamellas where the cations are octahedrally coordinated with OH^- forming layered structures, and anions are intercalated among the layers in order to balance their overall positive charge due to the partial substitution of M(II) with M(III).[59–61] The easy tunability of metal ions and the possibility to exchange the interlayer anions make LDHs attractive alternatives for applications in catalysis,[59,62–67] photocatalysis,[68–70] electrochemical oxygen evolution,[71,72] electrochemical sensors,[73–75] biology,[76] and separation processes.[77] Concerning their

application in catalysis, layered double hydroxides are mostly known as catalyst precursors for the reforming of methane toward syngas[78,79] and for the CO_2 hydrogenation to methane or methanol.[80,81]

Moreover, the interest for these compounds to be used as electrocatalysts for the electrochemical CO_2 conversion is recently increasing. However, since they are generally used in oxidation processes and have a relatively low electrical conductivity compared to metals, very few studies have been performed on the pristine LDHs as cathode materials. Nevertheless, in those papers, H_2, CO, and HCOOH were obtained as major products. Li et al.[82] reported a comparison between a Cu/MgAl and a Au/MgAl LDH obtained by a co-precipitation method. The respective active component (Cu and Au) was added by two different routes: copper was added to the LDH through a pre-intercalation of EDTA, while gold was added by an ion exchange process. Once the inks of the catalysts were obtained, they were loaded on a bulk glassy carbon electrode (1.8 cm^2). The catalytic performances for the CO_2ER were investigated in two different electrolytes ($KHCO_3$ and alcohol amine solution, containing ethanolamine and diethanol amine). Applying a fixed potential starting from -0.3 to -0.5 V vs RHE to the Cu/MgAl LDH and from -0.45 to -0.7 V vs RHE to the Au/MgAl LDH in $KHCO_3$, the Authors obtained a large variety of products, including H_2, CO, CH_4, and HCOOH. On the contrary, upon application of a potential in the same ranges to both LDHs in the alcohol amine solution, only gaseous products were obtained, i.e., H_2 and CO. Iwase et al.[83] reported the use of a bimetallic layered double hydroxide made of Cu and Al, obtained by a co-precipitation method and loaded on a carbonaceous gas diffusion layer (1.89 cm^2). The electrocatalyst, tested in a gas diffusion electrode set-up[84] under galvanostatic conditions (50 mA), led to the production of CO, HCOOH, and H_2 as major products and ethylene and ethanol as minor ones. Overall, these works demonstrated the possibility to use either ternary and binary Cu-based layered double hydroxides as electrocatalysts for the CO_2ER. However, both syntheses were based on complex and time-

consuming co-precipitation methods, at relatively high temperatures, that require further processing to load the LDHs on the conductive support. Moreover, they mainly displayed productivity toward C_1 products with relatively scarce selectivity.

In this work, nanostructured CuMgAl LDHs-based materials have been electrochemically synthesized on a large (4 cm^2) carbonaceous gas diffusion membrane made of carbon fibers (CP) for CO_2ER applications [85]. The morphology of the resulting material was thoroughly investigated by Scanning Electron Microscopy (SEM), Field Emission Gun-Scanning Electron Microscopy (SEM-FEG), Energy-dispersive X-ray spectroscopy (EDS), X-Ray diffraction and Raman spectroscopy proving that, through a simple, one-step, and highly reproducible potentiodynamic procedure, it was possible to obtain a composite material with intimate contact between the CuMgAl LDH and Cu^0/Cu_2O species. The electrocatalytic properties of the composite were studied during potentiostatic CO_2ER in liquid phase ($KHCO_3$) by evaluating the effect of the catalyst composition, particularly (i) different molar ratios between divalent and trivalent cations, (ii) different amount of loaded catalyst on the carbonaceous support, and (iii) different ratios between each cation, on the resulting catalytic performances. For the sake of brevity, the investigated materials will be named indicating the molar ratios among cations in the electrolytic solution used for their electrodeposition. The optimized catalyst, i.e., CuMgAl 2:1:1 LDH/CP, reached a productivity in acetic acid of 2.0 mmol g_{cat}^{-1} h^{-1} at a low applied potential (-0.4 V vs RHE) [41,86,87]. This unprecedented result demonstrates the beneficial effects of a composite combining the layered double hydroxide structure with highly dispersed copper species, which allows to obtain (i) a C_2 product at a low potential applied during CO_2ER, (ii) a selectivity close to 100% as to the CO_2 reduction products, since only H_2 as side product was detected in the gaseous phase, and (iii) an enhanced productivity compared to the nanostructured Cu^0/Cu_2O films investigated in our previous work.[17]

2. Results and Discussion

2.1. CuMgAl Layered Double Hydroxide electrodeposited on gas diffusion membranes

The electrodepositions of the Cu-containing LDH films over the carbonaceous support were carried out with a potentiodynamic method (Cyclic voltammetry, CV).[88] During the catalyst optimization, the role of both the cations molar ratios inside the electrolytic bath (see Paragraph 2.2.1) and the number of the deposition cycles (see Paragraph 2.2.2) on the catalytic performances were investigated. Before each deposition, the carbonaceous membrane was pre-treated following an already published process.[17] The results reported in this section are referred to the CuMgAl 2:1:1 LDH/CP, chosen as a representative benchmark of all the Cu-containing LDH samples synthesized in this work.

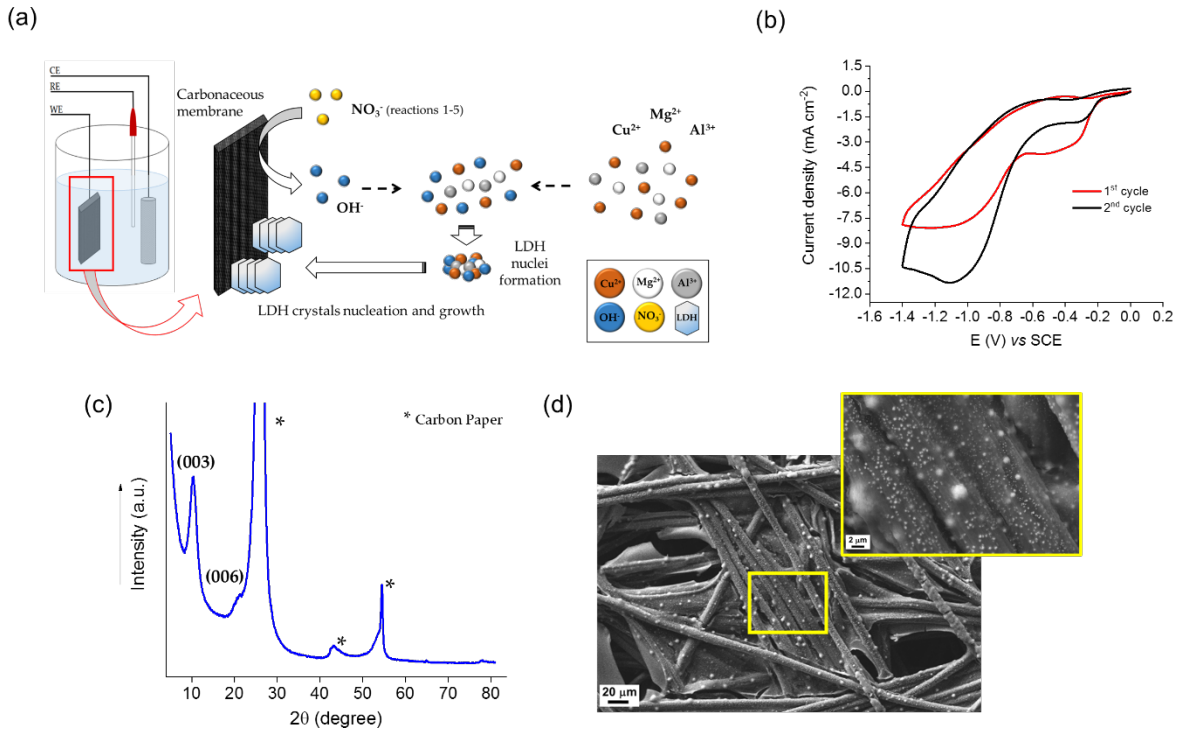

Figure 1. (a) Scheme of the processes occurring at the working electrode; (b) Example of a potentiodynamic deposition of the Cu-containing LDH films over the carbonaceous gas diffusion electrode; (c) X-ray diffraction pattern and (d) SEM images of a CuMgAl 2:1:1 LDH/CP electrodeposited film.

During the electrodeposition of the layered double hydroxide, which is schematically illustrated in **Figure 1**a, different reactions (1 – 5) take place involving, at the beginning, the reduction of nitrates coupled with the water reduction, which causes the consumption of H^+ ions and/or the generation of OH^-.

$$2H^+ + 2e^- \rightarrow H_2 \qquad E^0 = 0.0\,V \qquad (1)$$

$$NO_3^- + 2H^+ + 2e^- \rightarrow NO_2^- + H_2O \qquad E^0 = 0.93\,V \qquad (2)$$

$$NO_3^- + 10H^+ + 8e^- \rightarrow NH_4^+ + 3H_2O \qquad E^0 = 0.36\,V \qquad (3)$$

$$2H_2O + 2e^- \rightarrow H_2 + 2OH^- \qquad E^0 = -0.83\,V \qquad (4)$$

$$NO_3^- + H_2O + 2e^- \rightarrow NO_2^- + 2OH^- \qquad E^0 = 0.01\,V \qquad (5)$$

The hydroxide ions thus generated diffuse toward the bulk solution, while the cations species present in the electrolytic bath diffuse toward the electrode surface, forming the LDH nuclei. Once the amount of produced OH^- equalizes the one removed by the cations precipitation, the nucleation and growth of the crystals occur at the electrode surface. The rate of the LDH precipitation strongly depends on the presence of defects on the electrode surface, which act as nucleation centers, and on the oversaturation degree of the solution.[88] The voltammograms recorded during the electrodeposition process of the CuMgAl LDH, displayed in Figure 1b, show the presence of two cathodic peaks: one at -0.40 V, slightly anticipated at -0.28 V in the second cathodic sweep segment, and the other at -1.03 V. By comparing the deposition curves recorded with and without the Cu^{2+} species in the electrolytic bath, shown in Figure S1, it is worth noting that, while the most cathodic peak is present in both the MgAl LDH/CP and the CuMgAl LDH/CP electrodepositions, the first peak can be seen only in the Cu-containing electrolytic solutions. Thus, it can be stated that the peak at -0.40 V is ascribable to the reduction of copper ions. Moreover, it was observed that the current related to this peak decreases after the first deposition cycle (Figure 1b), while that associated to the peak at -1.03 V strongly increases.

Therefore, we can assume that a partial reduction of the copper species occurs as soon as the cathodic potential is applied, so hindering in some way, the reduction of nitrates which is favored during the second deposition cycle on the CP electrode modified with metal copper. The presence of Cu was also confirmed by CV characterization in basic solution (Figure S2), showing the typical redox waves associated to the different Cu species.[17,89] The less cathodic peak recorded during the second scan is associated with the deposition of copper onto a film already present on the conductive support, according to the literature evidences for Pt and stainless steel.[90] To assess the morphology and the chemical nature of the electrodeposited material, XRD, SEM, and Raman analyses were carried out.

The first evidence of the formation of the layered double hydroxide structure was given by the X-ray diffraction analysis (Figure 1c) that shows the main diffractions typical of the LDH phase, containing NO_3^- as interlayer anion, at 10.4° and 21.2° (2θ), and indexed as (003) and (006) reflections, respectively.[59,63] The Bragg angle of reflection (003) was used both to calculate the perpendicular dimension of the crystallites[91] and the relevant d-spacing. Such values are reported in the paragraphs describing the compositions investigated for each LDH (2.2.1 and 2.2.3). However, from the X-ray diffraction analysis alone it was not possible to confirm the ternary nature of the electrodeposited LDH. Moreover, the SEM picture reported in Figure 1d highlights that, after electrodeposition of the LDH, the carbon fibers of the support are homogeneously covered by a micro and nano structured coating exhibiting different morphological features. Further investigations were performed by EDS and SEM-FEG imaging of a freshly prepared CuMgAl 2:1:1 LDH/CP. SEM-FEG pictures are shown in **Figure 2**, while the EDS analyses are reported in Figures S3a and b.

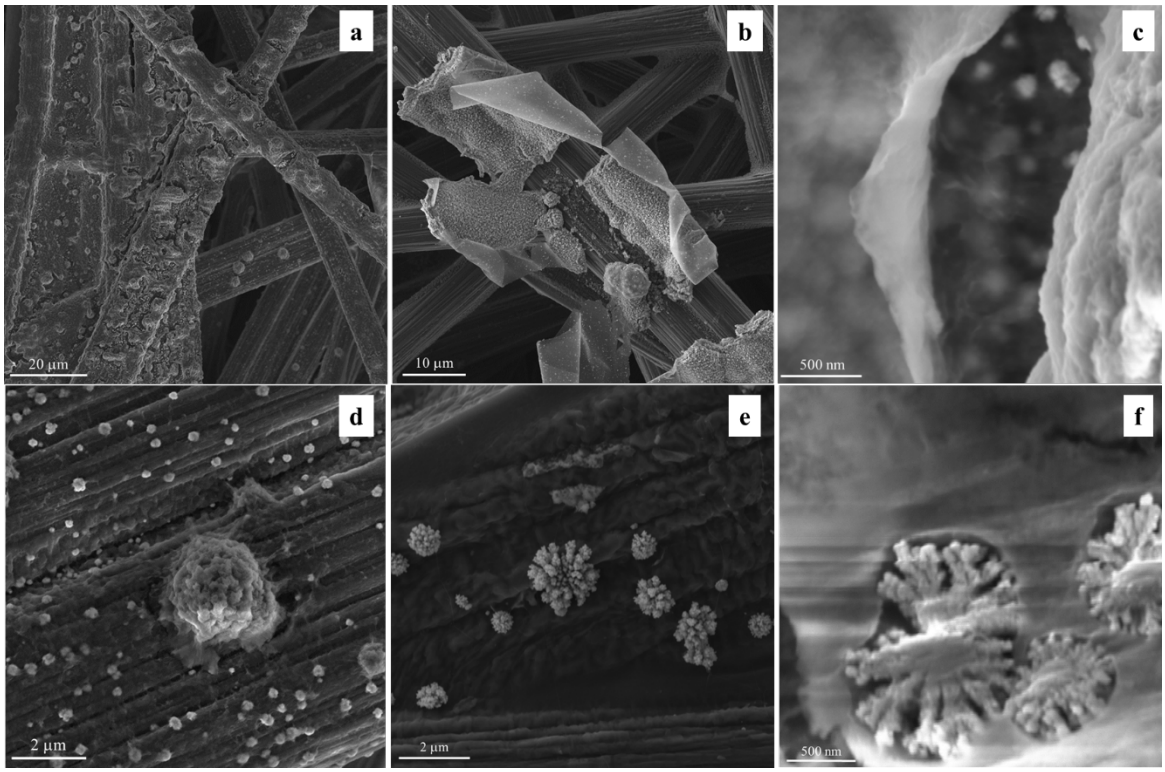

Figure 2. (a), (b), (c) SEM-FEG images of the layered deposit on the fibers; SEM-FEG images of the discrete particles with cauliflower-like (d) and coral-like (e, f) shapes

Figure 2a highlights the presence of a thin veil covering the superficial fibers, which was not evident from the SEM image shown in Figure 1d. Focusing on the thin film coating the fibers, the SEM-FEG pictures of a site where its continuity is interrupted are reported in Figure 2b and c, which clearly show its veil-like conformation with an estimated thickness of few tens of nm. Moreover, Figure S3a again highlights the layered nature of the fibers coating, which is a typical feature of the LDHs morphology.[92] The EDS analyses carried out in position 1 (Figure S3a) confirmed the ternary nature of the LDH with cations molar ratios of 1.4 for Cu/Mg, 1.8 for Cu/Al, and 1.3 for Mg/Al, and a total molar ratio between divalent and trivalent cations of 3.0, thus suggesting a very good match with the expected 2:1:1 ratio. Cauliflower-like particles, which could be also ascribed to a typical LDH morphology,[93] were observed (Figure 2d) where Cu, Mg and Al were detected by punctual EDS analysis and EDS mapping (Figure S5) without respecting the 2:1:1 ratio (cations molar ratios of 0.60 for Cu/Mg, 1.5 for Cu/Al and 2.5 for Mg/Al), thus suggesting the deposition of a LDH different

in composition. Moreover, in addition to the LDH veil and cauliflower-like particles, Figures 2c-f show the presence of other discrete particles with different morphologies that are located both on the fibers and incorporated in the LDH pores.

In particular, the smallest round particles decorating the fibers in Figure 2d were found to consist of Cu only, by EDS analysis.

Differently, in the coral-like particles in Figure 2e, Cu/oxidized Cu species were detected (Figure S3b), as the EDS analysis also showed a significant atomic percentage of oxygen. To further investigate the chemical nature of the coral-like structures, Raman analysis was carried out along the fiber (Figure S4a) and at a coral-like particle (Figure S4b). The results were consistent with the presence of Cu_2O species, displaying the typical peaks at 142, 214 and 626 cm^{-1} [17,94] at the particle. On the contrary, the analysis performed along the fibers shows the characteristic peak of the NO_3^- stretching,[95,96] remarking the presence of the layered double hydroxides veil with nitrate anions in the interlayer, together with the typical peaks related to the carbon fibers (1354 cm^{-1} "D-band" and 1581 cm^{-1} "G-band").[97]

As shown in Figure 2f and S3a, the coral-like particles were also found to be incorporated inside the LDH pores, and EDS analysis in position 2 of Figure S3a confirmed that they are made of Cu/oxidized Cu species, similarly to those spread over the fibers.

Then, Inductively Coupled Plasma - Atomic Emission Spectrophotometry (ICP-AES) analyses were carried out to investigate the ratio between Cu^0 and the oxidized Cu species present inside and outside the LDH structure, like Cu^{2+} and Cu^+. Exploiting the solubility of the Layered Double Hydroxides in acidic media, two identical CuMgAl 2:1:1 LDH electrocatalysts were solubilized in a 0.1 M HNO_3 solution. In this way, exploiting the oxidant nature of nitric acid, all the Cu species present in the materials (i.e., Cu^0, Cu^+ and Cu^{2+}) dissolved.

Other two samples were solubilized in a 0.01 M H_2SO_4, solution, which possesses only acidic properties, with the aim of dissolving only the oxidized Cu species (i.e., Cu^+ and Cu^{2+}).

As a result, the total concentration of Cu in the HNO_3 solution was found to be 193 ppm, while the overall amount of oxidized species in the H_2SO_4 solution was 165 ppm. By subtracting the second concentration from the first one, the concentration of copper coming from Cu^0 was 28 ppm, resulting in 15% of the total amount of Cu species. Therefore, the ratio between Cu^0 and the oxidized species is about 1:6.

These results confirm that the electrochemically synthesized material on CP fibers is composed of both ternary CuMgAl LDH and different copper-based particles. In particular, the electrodeposition process allowed to create an intimate contact among Cu/Cu_2O species and a ternary CuMgAl LDH.

2.2 Optimization of the CuMgAl electrocatalyst and catalytic tests performance

The optimization of the electrocatalyst formulation and properties was carried out by evaluating the following parameters: (i) molar ratio between total M(II) and M(III), (ii) amount of the loaded catalyst, and (iii) molar ratios among the three cations. Each electrocatalyst was tested during the liquid phase CO_2ER for a 1h reaction at -0.4 V vs RHE, especially to estimate the selectivity toward the production of acetic acid. The choice of these conditions was made on the basis of the outcomes of a previous work,[17] when acetic acid resulted the main liquid product and the differences in activity among the investigated catalysts were more evident.

2.2.1 Effect of the total M(II) and M(III) ratio

The first parameter investigated was the molar ratio between the divalent cations (Cu and Mg) and the trivalent one (Al). In fact, this parameter can deeply influence the catalytic activity of LDH and LDH-derived catalysts in different processes.[78,92,98,99] A set of electrocatalysts was

synthesized starting from two different electrolytic baths keeping a total molar concentration of 0.03 M:

I. M(II): M(III) = 6: 1, corresponding to the molar ratio Cu: Mg: Al = 3:3:1 (CuMgAl 3:3:1 LDH/CP)

II. M(II): M(III) = 3: 1, corresponding to the molar ratio Cu: Mg: Al = 1.5:1.5:1 (CuMgAl 1.5:1.5:1 LDH/CP)

The as prepared LDH films were investigated by SEM analyses (Figure S6). The 4 cm^2 area of the membrane was fully covered by the electrocatalyst in both cases, but the most homogeneous film was achieved by employing the latter cations composition.

Indeed, the 6:1 molar ratio led to a covering that appeared broken and scarcely attached to the carbon fiber. Contrarily, when using the 3:1 molar ratio, the material appeared more uniformly distributed along the fibers and the film well adherent to the CP.

Deeper investigations on the electrosynthesized LDH veil for each material were performed using SEM-FEG analysis. As shown in Figure S7, the electrodeposited LDH veils along the fibers have a porous structure. Interestingly, the 3:3:1 CuMgAl LDH presents a higher amount of incorporated coral-like particles and a new flat structure near the layered one which was subjected to further EDS investigations (see the following discussion).

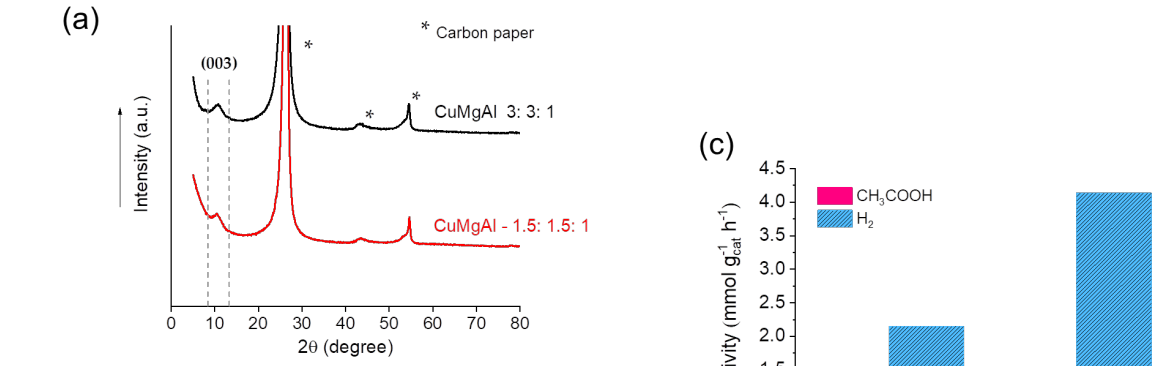

(b)

Cu^{2+}: Mg^{2+}: Al^{3+} (electrolytic bath)	Cu/Mg	Cu/Al	Mg/Al	M^{2+}/M^{3+}
3 : 3 : 1	0.7	1.9	2.8	4.7
1.5 : 1.5 : 1	1.0	1.2	1.2	2.4

Figure 3. XRD patterns of the electrosynthesized CuMgAl LDHs with different cations molar ratios (a); estimated total M(II)/M(III) ratio from EDS analyses (b); CO_2ER products distribution at -0.4 V vs RHE (1h reaction) for the two different LDH compositions (c).

Figure 3a and Figure S8 show the X-ray diffraction spectra of each sample and the presence of the layered double hydroxide structure is confirmed by the reflection peak indexed as (003), which shows a slight change in the 2θ position. In both cases, an average crystallites size of 19.5 nm was calculated by using the Scherrer formula from the full width at half maximum of (003) reflection peak, with a shape factor K=1.[100] Contrarily, the interlayer spaces, estimated by the angular position of the (003) reflection peak, obtained for the CuMgAl 3:3:1 LDH/CP was lower than the one relative to the CuMgAl 1.5:1.5:1 LDH/CP, e.g., 8.1 vs 8.8 Å, which are both typical values of the nitrate anions.[59] The reason for this difference was demonstrated by the studies carried out in 1983 by Miyata[101] and later by Marappa et al..[102]

Indeed, they both defined the increase of the interlayer spacing inside Mg/Al based layered double hydroxides containing NO_3^- as anion as a result of the increase of the *x* component in the general formula $[(M^{II})_{1-x}(M^{III})_x(OH)_2]^{x+}(A^{n-}_{x/n}) \cdot mH_2O]$, and thus of the increase of LDH layer positive charge.

The two papers reported that for a value of x = 0.3, the basal spacing increases up to 8.8 Å, while for lower values of x (i.e., x = 0.2) the basal spacing reaches values around 8.0 Å. Commonly, nitrate ions are shown to intercalate with their molecular plane inclined at an angle of ~ 70° to the metal hydroxide layer when the positive charge is high, due to the inclusion of a larger number of anions that have to pack closer together, whereas, when *x* is small, the plane formed by the NO_3^- results parallel to the basic layer. Therefore, concerning the two investigated LDHs, the increase of the interlayer space is in agreement with the increase of the molar fraction of Al^{3+}, which enhances the amount of negative ions (NO_3^- or CO_3^{2-}) required to balance the excess of positive charge.

Besides, the EDS analysis (Figure 3b) reports that the composition of the CuMgAl 1.5:1.5:1 LDH film is the one that better reflects that of the synthetic bath solution, confirming again that the best molar ratio between the total amount of M(II) and M(III) in this three-cations LDH is 3:1, in accordance with the literature.[92] Indeed, several inconsistencies were observed for the supposed 6:1 LDH. Although the X-ray diffraction analysis demonstrated again the presence of the layered double hydroxide structure, the EDS analysis achieved in position 3 (Figure S7) revealed the presence of several Cu/Al oxides species nearby the LDH structure where the estimated molar ratio among the cations did not match that of the electrolytic solution. Such evidences suggest the presence of a defective layered double hydroxide deposit over the carbon fibers, where the cations ratio approaches 4:1 or 5:1.

Therefore, it can be stated that using a higher molar ratio between divalent and trivalent cations in the electrolytic bath solution led to the formation of (i) a lower interlayer space, (ii) a defective LDH structure, and (iii) undesired oxides species.

Finally, in order to investigate the effect of the total cations molar ratio on the electrocatalytic performance, the two samples, with M(II):M(III) = 6:1 and 3:1, were tested for the liquid phase electrochemical CO_2 reduction (Figure 3c). Both electrocatalysts led to the production of acetic acid at -0.4 V vs RHE as the main liquid product but, the highest productivity was

achieved with the CuMgAl 1.5:1.5:1 LDH/CP that outperformed the other material by 5 times (1.5 vs 0.3 $mmol_{CH3COOH}$ g_{cat}^{-1} h^{-1}). The acetic acid productivities obtained with the LDHs with different total cations molar ratios were also normalized to the geometric area of the electrode (4 cm^2), obtaining 0.10 vs 0.42 $\mu mol_{CH3COOH}$ cm^{-2} h^{-1}, for the 6:1 and 3:1 ratio, respectively. This trend confirmed again the 3:1 total cations molar ratio as the one related to the most active material. Similarly, the H_2 production obtained with this electrocatalyst was about 60% higher than the 6:1 LDH (1.11 vs 0.70 μmol_{H2} cm^{-2} h^{-1}). Moreover, an evaluation of the Electrochemical Active Surface Area (ECSA) of the two LDHs was carried out. As a result, the ECSA values for the 6:1 and 3:1 LDHs were 9.4 $\pm$ 0.7 and 8.1 $\pm$ 0.7 cm^2, respectively.

Due to the same standard errors, the two ECSA values can be considered comparable. Therefore, although a higher ECSA is generally related to an electrode higher catalytic activity [103], in our case, other factors are responsible for the scarce performances displayed by the 6:1 LDH.

Indeed, these results comes from two main features, i.e., the final molar ratio in the electrocatalyst and the interlayer distance. On the one hand, the 3:1 molar ratio used in the electrolytic bath solution led to the formation of a more controlled LDH structure, as the mean ratio in the deposited material reflected the one of the solution. On the other hand, a higher interlayer space obtained with the 3:1 LDH could favor the diffusion of the carbon dioxide inside the structure. This phenomenon leads to the formation of a higher concentration of carbon sources in contact with the active phases, resulting in a higher production of acetic acid. Indeed, the presence of carbonates inside the LDH structure was confirmed by the X-ray diffraction analysis performed after the reaction, which will be discussed in the Paragraph 2.3. For these reasons, further optimizations of the material to be tested for CO_2ER were carried out employing 3:1 as the molar ratio between the total M(II) and the M(III).

2.2.2 Effect of the amount of the loaded catalyst

Once the best molar ratio between M(II) and M(III) was identified, the effect of different amounts of electrocatalyst loaded on the carbonaceous membrane was explored. In this case, the electrocatalyst composition, CuMgAl 1.5:1.5:1 LDH/CP was investigated by varying the numbers of deposition cycles.

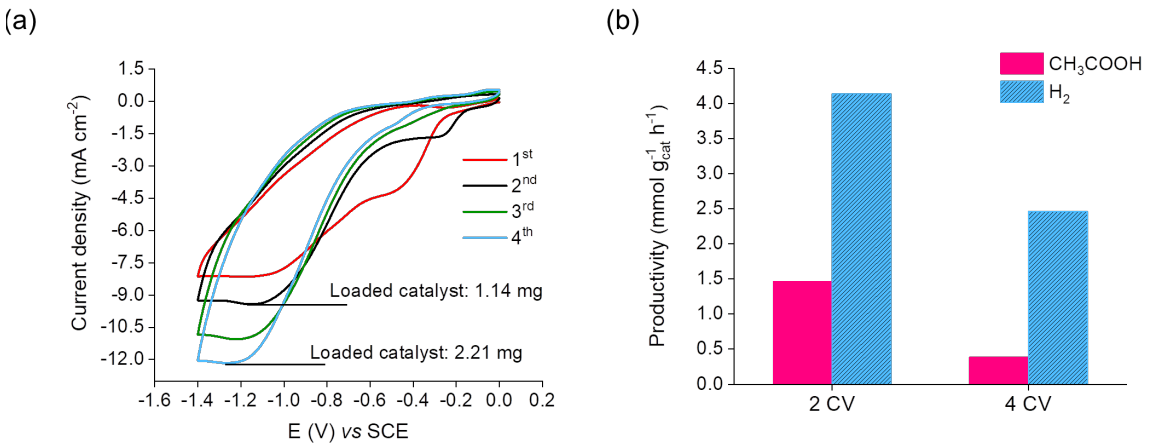

Figure 4. Current densities recorded during the electrodeposition processes (a); CO_2ER products distribution at -0.4 V vs RHE (1h reaction) for the different amounts of loaded catalyst (b).

Figure 4a shows that increasing the numbers of CV cycles, the amount of loaded catalyst proportionally increased with the current density. A mass increment of 94% was observed between the second and the fourth electrodeposition cycle (1.14 vs 2.21 mg).

By comparing the outcomes of the catalytic tests, it can be noticed that a higher productivity per gram of catalyst was obtained by the sample on which the lower amount of electrocatalyst was loaded (Figure 4b). Indeed, the selective applied potential led again to the formation of acetic acid as the main liquid product and the productivity values obtained with the two loading were 1.5 vs 0.4 mmol g_{cat}^{-1} h^{-1}. The presence of a ticker layer of LDH containing a higher amount of non-redox active centers (Mg and Al) produced a less conductive material where the charge transfer from the conductive support to the active redox species (Cu) is likely to be hindered, and the H^+ diffusion toward the electroactive surface area of the electrode is limited, thus resulting in a decrease of the catalytic activity. Indeed, after the

second cycle of deposition, the peak related to the nitrate reduction started to increase at the expense of the peak related to copper deposition that slowly disappeared, suggesting the prevalent formation of the ternary LDHs.

In this way, the coral-like Cu^0/Cu_2O particles are likely more covered by non-redox active species (Mg and Al) and this causes a change at the electrode/electrolyte interface that affects negatively the catalytic activation processes. [[104,105]An evaluation of the ECSA was carried out for both electrocatalysts, finding out that the one obtained with 4 CVs displayed a lower ECSA than the material synthesized with 2 CVs (4.6 ± 0.4 vs 8.1 ± 0.7 cm^2). Such a result is consistent with the lower catalytic activity displayed by the 4 CV sample.

For a better comparison, the productivities of acetic acid and H_2 were also normalized to the geometrical surface area of the CP, since a different amount of the loaded catalyst may amplify the difference between the productivities. As shown in **Table 1**, regardless of the amount of loaded catalyst, the material obtained with 2 CVs of electrodeposition displayed the highest amount of acetic acid while reducing the amount of H_2 evolution. Such a behavior is consistent with the evaluated values of ECSA.

Table 1. Productivities normalized to the geometrical area (4 cm^2) of the CuMgAl 1.5:1.5:1 LDH/CP electrocatalyst obtained with 2 and 4 CVs.

Number of CVs	*CH_3COOH ($\mu mol\ cm^{-2}\ h^{-1}$)*	*H_2 ($\mu mol\ cm^{-2}\ h^{-1}$)*
2	0.42	1.11
4	0.20	1.29

Therefore, the 2 cycles electrodeposition was chosen for the preparation of CuMgAl 1.5:1.5:1 LDH/CP and the sample was employed for further optimizations.

2.2.3 Effect of the Cu/Mg/Al molar ratios

Lastly, a set of CuMgAl LDHs where the total M(II)/M(III) molar ratio was 3:1 was prepared using 2 deposition cycles to investigate the effect of the molar ratios among cations. Three different synthetic bath solutions were employed for the electrosynthesis of the catalysts, and precisely:

I. Cu^{2+}: Mg^{2+}: Al^{3+} = 1: 2: 1, corresponding to a theoretical CuMgAl 1:2:1 LDH/CP

II. Cu^{2+}: Mg^{2+}: Al^{3+} = 1.5: 1.5: 1, corresponding to a theoretical CuMgAl 1.5:1.5:1 LDH/CP

III. Cu^{2+}: Mg^{2+}: Al^{3+} = 2: 1: 1, corresponding to a theoretical CuMgAl 2:1:1 LDH/CP

(a)

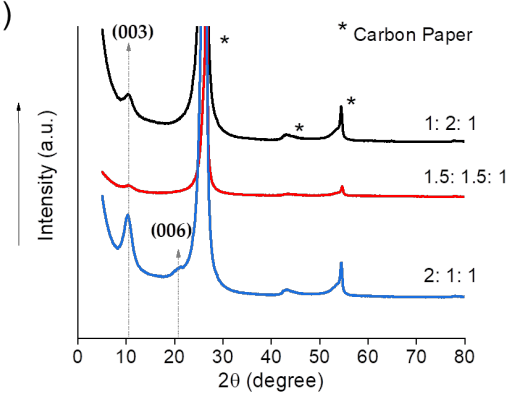

(b)

Cu^{2+}: Mg^{2+}: Al^{3+} (electrolytic bath)	Cu/Mg	Cu/Al	Mg/Al	M^{2+}/M^{3+}
1 : 2 : 1	0.4	1.0	2.6	3.6
1.5 : 1.5 : 1	1.0	1.2	1.2	2.4
2 : 1 : 1	2.2	2.0	0.9	2.9

Figure 5. (a) XRD patterns of the CuMgAl LDHs with different cations ratios; (b) Estimated cations ratios from EDS analyses on the electrosynthesized films.

X-ray diffraction analyses were carried out (**Figure 5**a). All spectra show the typical reflection at 10.4° (2θ) indexed as (003) with no change in the position of the Bragg's angle, a feature ascribable to the similar ion radius of Mg^{2+} (0.72 Å) and Cu^{2+} (0.73 Å).[106]

However, it is worth noting that the intensity of the reflection (003) for the 2:1:1 sample was the highest, compared to the other materials, and it is the only case in which it was also possible to observe the second order reflection (006), thus suggesting a higher crystallinity of this LDH. The obtained d-spacing value was always 8.5 Å, since the amount of Al was the

same for all samples and the different ratio of the divalent cations did not influence the d value to a significant extent (see discussion in Paragraph 2.2.1).

A substantial difference among the films was found in the crystallite size and in the estimated ratios obtained by the EDS analyses.

The average crystallite dimensions calculated considering the reflection at 10.4° (2θ), for the CuMgAl 1:2:1, CuMgAl 1.5:1.5:1, and CuMgAl 2:1:1 were 120.9, 19.5, and 9.9 nm, respectively. This trend was also confirmed by the SEM analyses (Figure S9), which not only showed the presence of a very homogeneous covering along the fibers with well dispersed particles in all three electrocatalysts, but also clearly displayed a decrease in the particles sizes by increasing the amount of copper inside the electrolytic solution. Moreover, the estimated molar ratios among Cu/Mg/Al and between the total amount of M(II) and M(III) obtained with the EDS analyses (Figure 5b) pointed out that the CuMgAl 2:1:1 LDH/CP catalyst exactly reflected the composition of the electrolytic bath solution unlike the other two LDHs. Only by providing a double amount of copper, the nominal ratio was maintained.

Finally, the as obtained electrocatalysts were tested for the liquid phase CO_2ER (**Figure 6**) in order to choose the best electrocatalyst in terms of activity.

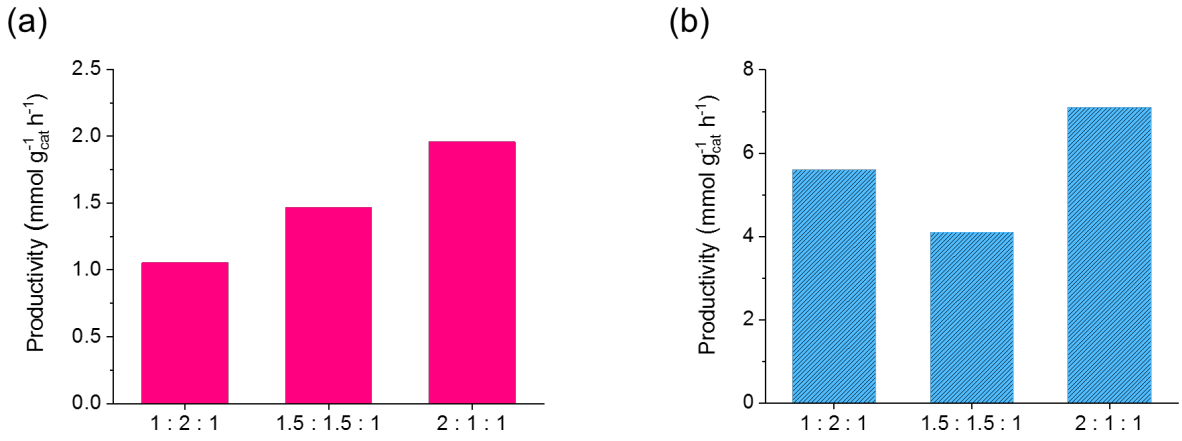

Figure 6. CH_3COOH production (a) and hydrogen production (b) at -0.4 V vs RHE (1h reaction)

Again, the CO_2 reduction tests led to the selective formation of acetic acid, but significant results were obtained concerning the productivity. Indeed, the greatest production of CH_3COOH was obtained by the electrocatalyst that displayed the most crystalline structure and the lower sizes of the crystallite. In particular, the production increased from a value of 1.1 $mmol_{CH3COOH}\ g_{cat}^{-1}\ h^{-1}$ obtained with the CuMgAl 1:2:1 LDH/CP catalyst up to 2.0 $mmol_{CH3COOH}\ g_{cat}^{-1}\ h^{-1}$ obtained with the CuMgAl 2:1:1 LDH/CP. Again, the productivities were also calculated in respect to the geometric area of the electrode. As a result, the CuMgAl 1:2:1 LDH showed a productivity of 0.33 μmol $cm^{-2}\ h^{-1}$ while the CuMgAl 2:1:1 LDH displayed a value of 0.53 μmol $cm^{-2}\ h^{-1}$, so confirming the same trend of acetic acid production, as discussed previously. Moreover, since the acetic acid was the only detected CO_2 reduction product (Figure S10), the Faradaic Efficiency (FE) values were calculated referring to this compound for the CuMgAl 1:2:1, 1.5:1.5:1, and 2:1:1 LDHs, and resulted 33 %, 41 %, and 84 %, respectively. Such a result confirmed that the CuMgAl 2:1:1 LDH catalyst provides not only the highest productivity in acetic acid, but also the highest selectivity and it is capable of driving the supplied energy toward the formation of the desired product. Hydrogen was the only gaseous compound detected (Figure S11), with a productivity of 1.88 and 1.51 μmol $cm^{-2}\ h^{-1}$ for 1:2:1 and 2:1:1 LDHs, respectively. **Table 2** shows the current densities recorded during the CO_2ER employing the three LDHs containing different cations molar ratios and their ECSA values. As it can be noticed the highest current density was recorded for the CuMgAl 2:1:1 LDH which displayed an ECSA twice greater than that exhibited by the other two materials.

Table 2. Current densities recorded during the CO_2ER for the LDHs based on different cations molar ratios and their ECSA values

Electrocatalyst	*J (mA mg_{cat}^{-1})*	*ECSA ± STD error (cm^2)*
CuMgAl 1:2:1 LDH/CP	0.84	7.8 ± 0.8
CuMgAl 1.5:1.5:1 LDH/CP	1.00	8.1 ± 0.7
CuMgAl 2:1:1 LDH/CP	1.10	18.5 ± 0.8

As far as the acetic acid production is concerned it is reasonable to state that the higher is the molar ratio of Cu with respect to the other non-redox active species (Mg and Al), the higher is its production.

Overall, the results obtained highlight that:

I. The intimate contact between the ternary CuMgAl LDHs and the Cu^0/Cu_2O particles enhances the production of acetic acid. This suggests that the presence of the LDH structure increases the availability of the carbon sources at the surface and inside the electrocatalysts.

II. The higher interlayer space obtained with the total cations molar ratio of 3:1 is likely to favor the entrance of CO_2 inside the layered structures, thus enhancing the amount of carbonates species and the subsequent acetate production.

III. The higher amount of nano-sized particles and nanometric crystallite sizes, together with the higher crystallinity of the CuMgAl 2:1:1 LDH/CP led to the formation of a more active material.

IV. The higher amount of coral-like particles in CuMgAl 2:1:1 LDH/CP (Figure S9) suggests that the dominant presence of active Cu^+/Cu^0 redox couple species is capable to favorably drive the reaction pathway toward the C-C bond formation.

Finally, a comparison between the most promising electrocatalyst here described (i.e., CuMgAl 2:1:1 LDH) and the Cu-based catalysts reported in literature is given in **Table 3**.

However, the collection of the data was difficult due to the need for comparable experimental conditions, regarding the employment of a gas diffusion layer based on a carbonaceous material, the application of a fixed potential instead of a fixed current density, and a continuous CO_2 feed. Moreover, acetic acid is not a common product for the CO_2ER and the LDH-based electrocatalysts reported in literature only form C_1 products [82,83]. In the Table, the productivities are reported in respect with the mass (per gram) of the loaded catalyst since it was not always possible to determine productivity in respect with the geometric area.

Table 3. Overview of the most recent CH_3COOH productivities obtained with Cu-based catalysts over carbonaceous GDL in liquid phase

Electrocatalyst	*Potential (V vs RHE)*	*Electrolyte*	*Productivity* (mmol g_{cat}^{-1} h^{-1})	*Reference*
Porous Cu^0 NPs	-0.9	0.1 M $KHCO_3$	1.20	[87]
Cu^0 NPs on CNT (impregnation)	~-0.8	0.5 M $KHCO_3$	0.21	[40]
Cu^0 NPs on CNT (Cu nanowires)	~ - 1.35	0.5 M $KHCO_3$	0.57	[41]
Cu_2O	~ -0.85	0.5 M $KHCO_3$	0.50	[50]
Cu^0	-0.4	0.3 M $KHCO_3$	0.056	[17]
Cu_2O-Cu^0	-0.4	0.3 M $KHCO_3$	0.31	[17]
CuMgAl 2:1:1 LDH	-0.4	0.3 M $KHCO_3$	2.00	This work [85]

It is evident that the CuMgAl 2:1:1 LDH/CP catalyst possesses the best acetic acid productivity while working at low cathodic potential.

2.3 Potentials screening using CuMgAl 2:1:1 LDH/CP and stability over time

To summarize, the Cu-containing LDH, synthesized by 2 electrodeposition cycles, having a molar ratio between M(II) and M(III) of 3:1 and ratios among cations of 2:1:1, was chosen as the optimized electrocatalyst. Therefore, a study of the different applied potentials during the CO_2ER and an evaluation of its stability over time were performed.

A potentials screening was carried out in order to estimate (i) the effective selectivity toward acetic acid at -0.4 V vs RHE, (ii) the possibility to obtain other reduction products from CO_2 by applying both a less cathodic potential and a more cathodic one. To this purpose, -0.2 and -0.8 V vs RHE were selected for the screening and the achieved results were compared with those obtained at -0.4 V vs RHE in the liquid phase CO_2ER.

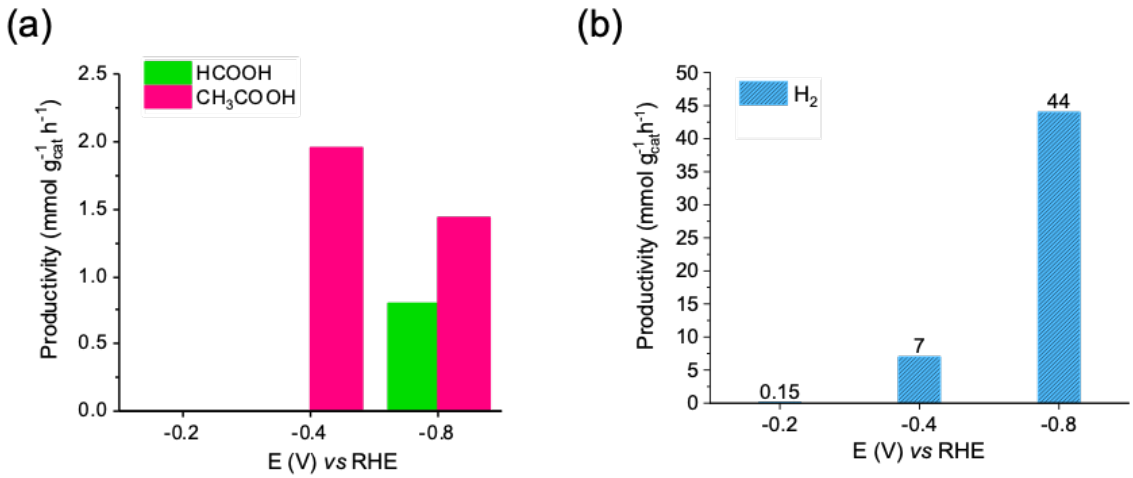

Figure 7. CO_2ER liquid (a) and gaseous (b) products distribution for a 1h reaction at different applied potentials using the CuMgAl 2:1:1 LDH/CP

The as obtained products distribution is shown in **Figure 7**. As a result, by applying the most cathodic potential (-0.8 V), the selectivity toward acetic acid was reduced and the formation of formic acid was pointed out. Moreover, as the potential was more cathodic, a higher amount of hydrogen was evidenced, so hindering the production of acetic and formic acids or of other reduction products. On the other hand, the reaction at -0.2 V vs RHE produced only a small amount of hydrogen.

However, the least cathodic applied overpotential was not enough for the reduction of carbon dioxide to start and no liquid products were detected. Therefore, -0.4 V vs RHE was again confirmed to be the most selective potential for the production of acetic acid in the liquid phase CO_2ER with the experimental set-up used in this work. The following considerations can be proposed to explain why the CuMgAl 2:1:1 LDH/CP electrocatalyst works better than the Cu_2O-Cu^0/CP (0.31 vs 2.0 $mmol_{CH3COOH}$ g_{cat}^{-1} h^{-1})., which up to date was considered by us the best performing material for the acetic acid production. The Cu containing LDH acts as a catalyst for the electroreduction of CO_2 in liquid phase, since it couples the presence of different active phases of copper with the basicity of the hydroxide itself, which likely favors the interaction with CO_2.[107] Moreover, the 3D structure of the carbonaceous gas diffusion membrane joined with the lamellar assembly of the LDH is able to favor the interaction of the CO_2 and its derived species at the electrode surface, also thanks to a dynamic exchange process occurring in the interlayers [108]. Furthermore, due to the higher affinity to carbonates,[82] the LDH can work as a concentrator for the CO_2 during the reaction.

In order to confirm the entrance of carbonates in the lamellar structure and if the crystallinity was maintained after a 1 h reaction at -0.4 V vs RHE, X-ray diffraction analysis was also recorded right after the reaction (Figure S12). The diffraction pattern shows the presence of a broad reflection indexed as the basal (003), confirming the maintenance of the structure, while the (006) reflection disappears. However, the intensity of the 003 reflection was lower than the one recorded for the pristine LDH, thus suggesting a loss of crystallinity during the CO_2 reduction process, while the nanostructure of the electrocatalyst was preserved, since the average size of the crystallites only grew up from 9.9 nm to 25.6 nm. This slight change can be attributed to a sintering process which has been widely proved in the literature for nanoparticle dimensions < 25 nm.[109,110] It is also worth noting the shift of the Bragg angle of reflection (003) from 10.4° to 11.7° (2θ) and the decrease of the d-spacing from 8.5 Å to 7.6

Å, which is typical of the CO_3^{2-} interlayer anion, which confirms the effective adsorption/entrance of the carbon dioxide inside the LDH structure during the reaction.

Finally, the stability of the CuMgAl 2:1:1 LDH/CP electrocatalyst was studied over time at -0.4 V vs RHE. Figure S13 shows the recorded current density during a 24 h reaction and demonstrates no degradation of the sample, even if the catalyst had been working for a longer time, with a relative standard deviation per hour (% RSD h^{-1}) of 0.54 associated to the average J_{tot} value. Moreover, the LDH structure stability after the 24 h reaction was evaluated by means of X-ray diffraction analysis (Figure S14). The reflection (003) at 11.8° (2θ) confirmed the presence of the LDH with CO_3^{2-} as the interlayer anion, thus highlighting the stability of such a structure upon application of –0.4 V vs RHE for longer times than 1 h. The shift of the (003) reflection, in respect with the value recorded when nitrate is the interlayer anion, was already visible after 1 h reaction. Moreover, a reflection at 43.5° (2θ), that was not visible in the XRD pattern recorded after 1 h reaction, stands out from the reflections of the support and it can be referred to Cu^0. Such an evidence highlights the presence of metal copper after 24 h reaction, which may derive from both a reduction of a small fraction of the initial Cu oxides species and an increase of its crystallinity. For the sake of clarity, the peak at 18.3° (2θ), which is also visible in Figure S8, can be attributed to the carbonaceous support.

3. Conclusion

Outstanding performances toward the electrochemical CO_2 reduction were obtained by using new CuMgAl LDHs based materials. We successfully demonstrated the possibility to exploit the layered double hydroxides, generally used as catalyst precursors and widely proven to be active in oxidation processes, even in a reduction reaction. Unlike the LDHs already reported in the state of the art[82,83] that are obtained by the standard co-precipitation methods, the materials here designed were directly achieved on a carbonaceous gas diffusion membrane by means of simple, low time-consuming, and highly reproducible electrochemical deposition.

Such a procedure, carried out at ambient temperature and pressure, allowed to obtain fully covered 4 cm^2 sized membranes with homogeneous films well adherent to the carbon fibers. Moreover, the morphology of each electrocatalyst was thoroughly investigated and it was proven the existence of a composite material with an intimate contact between a nanostructured ternary CuMgAl LDH in the form of layered veils and cauliflower-like particles and Cu^0/Cu_2O species, in the form of coral-like particles. Several parameters were investigated to obtain the most active electrocatalyst composition by evaluating the performances in terms of acetic acid productivity during a potentiostatic CO_2 reduction at -0.4 V vs RHE for 1h, which were already demonstrated to be a selective potential and the best reaction time.[17] As a result, all catalysts displayed selectivity toward the production of acetic acid, concerning the liquid products and the highest activity was obtained by employing the CuMgAl 2:1:1 LDH/CP, outpacing the previous results obtained with the Cu_2O-Cu^0/CP electrocatalyst.[17]

Such a result demonstrates that, by virtue of their high design flexibility, the presence of many basic sites, and the high affinity toward carbonate anions, LDHs, alone or coupled with different copper active phases, may become emerging materials capable to produce high added-value commodities with optimum productivities in the electrochemical CO_2 reduction.

4. Experimental Section

Chemicals and materials: Nafion membrane N-115 (0.125 mm thick, ≥ 0.90 meq/g exchange capacity), Toray Carbon Paper (TGP-H-60), magnesium nitrate hexahydrate ($Mg(NO_3)_2 \cdot 6H_2O$), and copper tape were purchased from Alfa Aesar. Copper nitrate trihydrate ($Cu(NO_3)_2 \cdot 3H_2O$), aluminum nitrate nonahydrate ($Al(NO_3)_3 \cdot 9H_2O$), sulfuric acid (96% - 98%), nitric acid (> 65%), sodium hydroxide, ethanol (96.0 – 97.2%), potassium hydrogen carbonate, and phenol were purchased from Sigma-Aldrich. Deuterium oxide (99.96%) was purchased from

Eurisotop. Pure carbon dioxide (≥ 99.9%) was acquired by Rivoira S.r.l.. Gas sampling bags (Tedlar Bags) were obtained from Supelco. All chemicals were of reagent grade or higher.

Apparatus: The electrodeposition of the layered double hydroxides was carried out in a conventional three-electrode cell connected to a potentiostat (CH Instrument 660 C). 4 cm^2 sized Toray Carbon Paper (CP) and a Pt gauze were used as the working and counter electrodes, respectively. Electrode potentials were referred to an aqueous saturated calomel electrode (SCE), with the exception of the electrocatalytic tests for which the potentials were quoted to the reversible hydrogen electrode, RHE. The morphology and the structure of the electrocatalysts were investigated by SEM and SEM-FEG analyses using the E-SEM Zeiss EVO 50 Series instrument and a LEO 1530 ZEISS instrument equipped with Schottky emitter and an "In-lens" detectors for secondary electrons imaging. EDS measurements were performed with an Oxford INCA system equipped with a 30 mm^2 Silicon Drift Detector and a Brucker Quantax 200 Detector. X-ray diffraction analyses (XRD) were carried out using a PW1050/81 diffractometer (Philips/Malvern, Royston, UK) coupled with a graphite monochromator in the diffracted beam and controlled by a PW1710 unit (Cu Kα, λ = 0.15418 nm) and a PANalytical X'Pert PRO diffractometer equipped with a fast solid state X'Celerator detector. Cu Kα radiation was used (λ=0.15418 nm) at 40 mA, 40 kV. The 2θ range was investigated from 3.5° to 80° with a step size of 0.066° and time/step of 300 s. Raman spectra were recorded with a micro-spectrometer Raman RM1000 (Renishaw/Thermo Fisher, New Mills, Wotton-under-Edge, Gloucestershire, UK) equipped with a Leica DMLM optical microscope and a CCD detector. The excitation wavelength came from an Ar^+ laser (λ = 514.5 nm) with an output power of 25 mW. This power was reduced as needed by neutral density filters in order to prevent the sample damage. The electrochemical CO_2 reduction reaction tests were carried out in a two-compartment electrochemical (H-type) cell (Pine Research Instrumentation, Inc.). The carbonaceous membranes (CP) coated with the

electrocatalysts were used as the working electrodes, while a Ag/AgCl (KCl sat.) electrode and a Pt gauze were used as the reference and counter electrodes, respectively. Gaseous products were detected by a Thermo Focus GC (TCD detector) with a carbon molecular sieve column (CARBOSPHERE 80/100 6' x 1/8''). ^{1}H-NMR spectra were recorded by means of an Inova 600 spectrometer (600 MHz) coupled with a Triple Resonance Probe.

Pretreatment of the carbonaceous support: A geometrical surface area of 4 cm^2 of Toray carbon paper was cut out from a 19 x 19 cm foil. The optimization of the pretreatment procedure was described in a previous work.[17] Each piece of the carbonaceous membrane was soaked in 1 M H_2SO_4 for 2 h, followed by a 1 h treatment in pure EtOH. Finally, the membranes were rinsed with distilled H_2O and dried until reaching a constant weight. The carbonaceous support was also named gas diffusion layer (GDL).

Electrodeposition of CuMgAl Layered Double Hydroxides on the carbon paper electrode:

The three-metals LDHs films were deposited on the cleaned carbonaceous supports by adapting an already reported procedure.[88,92,95] Different freshly prepared 0.03 M solutions containing the nitrate salts of Cu^{2+}, Mg^{2+}, and Al^{3+} were obtained by varying the ratio between the total moles of the divalent metals and those of the trivalent metal, whose optimization was discussed in Paragraph 2.2.1.

A variable potential from 0.0 to -1.4 V was applied with a scan rate of 30 mV s^{-1}. The as-obtained Cu-containing LDH thin layer was thoroughly rinsed in distilled H_2O and dried to a constant weight. As already stated in the Introduction part, the materials are named indicating the molar ratios among cations in the electrolytic bath solution used for the electrodeposition.

Electrochemical characterization: The determination of the Electrochemical Active Surface Area (ECSA) was carried out varying the scan rate of different cyclic voltammetries (25, 50, 100, 200, 300 mV s^{-1}) recorded around -0.7 V vs SCE ($\pm$ 10 mV), which is a potential at which the electrocatalysts displayed a capacitive current (Figure S2). The CVs were carried out in 1 M NaOH and the ECSA was calculated dividing the double-layer electrochemical

capacitance (C_{dl}) by the specific capacitance of the sample (0.040 mF cm^{-2} for the carbonaceous materials [111]. All the ECSA values are reported with the standard error (STD error = $\sigma/\sqrt{N}$).

ICP-AES analyses: The Inductively Coupled Plasma - Atomic Emission Spectrophotometry analyses were carried out by an Agilent 4210 MP-AES Atomic Emission Spectrometer.

To this aim, the CuMgAl 2:1:1 LDH was solubilized in two acidic solutions, i.e., 0.01 M H_2SO_4 and 0.1 M HNO_3. In particular, two samples of CuMgAl 2:1:1 LDH were electrosynthesized and solubilized in 5 mL of each acidic solution at 318 K, stirring gently. Starting from 1000 ppm standard solutions of each cation, five standards were prepared (5, 10, 25, 50, 100 ppm) and the calibration lines of the three cations were recorded prior to the samples investigation.

Electrocatalytic tests: The liquid phase CO_2 electrochemical reduction tests were performed in a H-type cell whose setup was described elsewhere.[17] A 0.3 M $KHCO_3$ solution was employed as the supporting electrolyte (pH = 8.30). The cathodic side was pre-saturated with a constant flux of pure CO_2 (20 mL min^{-1}) for 30 min and then maintained at 5 mL min^{-1} during the reaction. All the applied potentials used for the CO_2ER were referred to the RHE. The liquid products were analyzed by a quantitative ^{1}H-NMR analysis, adding phenol as the internal standard and deuterium oxide to provide an internal lock signal. Gaseous products developed during the electrocatalytic tests were collected in a gas sampling bag and analyzed by gas chromatography.

Supporting Information

Supporting Information is available from the Wiley Online Library or from the author.

Acknowledgements

This work was supported by the Emilia-Romagna region POR FSE 2014/2020, the three-year plan "High Skills for Research, Transfer Technology and Entrepreneurship", project "Power to fuels: electrocatalytic reduction of CO_2 to methane and alcohols".

The manuscript was written through contributions of all authors. All authors have given approval to the final version of the manuscript.

Conflict of interest

The Authors declare no conflict of interest

Data Availability Statement

The data that support the findings of this study are available from the corresponding authors upon reasonable request.

References

[1] T. R. Karl, K. E. Trenberth, *Science (80-.).* **2003**, *302*, 1719.

[2] CO_2 Levels: Current and Historic Atmospheric Carbon Dioxide/Global Temperature Graph and Widget.

[3] H. Wang, Y. Liu, A. Laaksonen, A. Krook-Riekkola, Z. Yang, X. Lu, X. Ji, *Renew. Sustain. Energy Rev.* **2020**, *131*, 1.

[4] R. K. Pachauri, L. A. Meyer, Core Writing Team, *IPCC, 2014: Climate Change 2014: Synthesis Report. Contribution of Working Groups I, II and III to the Fifth Assessment Report of the Intergovernmental Panel on Climate Change*, Geneva, Switzerland, **2014**.

[5] The Royal Society, *Dealing with carbon dioxide at scale*, **2017**.

[6] E. Ruiz-López, J. Gandara-Loe, F. Baena-Moreno, T. R. Reina, J. A. Odriozola, *Renew. Sustain. Energy Rev.* **2022**, *161*, 1.

[7] C. Ampelli, C. Genovese, B. C. Marepally, G. Papanikolaou, S. Perathoner, G. Centi, *Faraday Discuss.* **2015**, *183*, 125.

[8] J. Shi, Y. Jiang, Z. Jiang, X. Wang, X. Wang, S. Zhang, P. Han, C. Yang, *Chem. Soc. Rev.* **2015**, *44*, 5981.

[9] S. Sultana, P. Chandra Sahoo, S. Martha, K. Parida, *RSC Adv.* **2016**, *6*, 44170.

[10] J. Grodkowski, P. Neta, *J. Phys. Chem. B* **2001**, *105*, 4967.

[11] S. Roy, A. Cherevotan, S. C. Peter, *ACS Energy Lett.* **2018**, *3*, 1938.

[12] G. Galletti, P. Prete, S. Vanzini, R. Cucciniello, A. Fasolini, J. De Maron, F. Cavani, T. Tabanelli, *ACS Sustain. Chem. Eng.* **2022**, *10*, 10922.

[13] A. Waldvogel, A. Fasolini, F. Basile, S. Thomas, A.-C. Roger, *Energy & Fuels* **2021**, *35*, 13304.

[14] S. N. Habisreutinger, L. Schmidt-Mende, J. K. Stolarczyk, *Angew. Chemie Int. Ed.* **2013**, *52*, 7372.

[15] S. Rej, M. Bisetto, A. Naldoni, P. Fornasiero, *J. Mater. Chem. A* **2021**, *9*, 5915.

[16] C. Genovese, C. Ampelli, S. Perathoner, G. Centi, *J. Catal.* **2013**, *308*, 237.

[17] M. Serafini, F. Mariani, A. Fasolini, E. Scavetta, F. Basile, D. Tonelli, *ACS Appl. Mater. Interfaces* **2021**, *13*, 57451.

[18] M. Bevilacqua, J. Filippi, H. A. Miller, F. Vizza, *Energy Technol.* **2015**, *3*, 197.

[19] L. Li, Y. Huang, Y. Li, *EnergyChem* **2020**, *2*, 1.

[20] S. Jin, Z. Hao, K. Zhang, Z. Yan, J. Chen, *Angew. Chemie Int. Ed.* **2021**, *60*, 20627.

[21] S. Bensaid, G. Centi, E. Garrone, S. Perathoner, G. Saracco, *ChemSusChem* **2012**, *5*, 500.

[22] A. U. Pawar, C. W. Kim, M.-T. Nguyen-Le, Y. S. Kang, *ACS Sustain. Chem. Eng.* **2019**, *7*, 7431.

[23] A. Kumar, V. Hasija, A. Sudhaik, P. Raizada, Q. Van Le, P. Singh, T.-H. Pham, T. Kim, S. Ghotekar, V.-H. Nguyen, *Chem. Eng. J.* **2022**, *430*, 1.

[24] O. G. Sánchez, Y. Y. Birdja, M. Bulut, J. Vaes, T. Breugelmans, D. Pant, *Curr. Opin. Green Sustain. Chem.* **2019**, *16*, 47.

[25] P. K. Jiwanti, S. Sultana, W. P. Wicaksono, Y. Einaga, *J. Electroanal. Chem.* **2021**, *898*, 115634.

[26] R. L. McCreery, *Chem. Rev.* **2008**, *108*, 2646.

[27] N. Yang, S. R. Waldvogel, X. Jiang, *ACS Appl. Mater. Interfaces* **2016**, *8*, 28357.

[28] Q. Zhai, Y. Pan, L. Dai, *Accounts Mater. Res.* **2021**, *2*, 1239.

[29] G. L. De Gregorio, T. Burdyny, A. Loiudice, P. Iyengar, W. A. Smith, R. Buonsanti, *ACS Catal.* **2020**, *10*, 4854.

[30] Z. Xing, L. Hu, D. S. Ripatti, X. Hu, X. Feng, *Nat. Commun.* **2021**, *12*, 1.

[31] H. Cui, Y. Guo, L. Guo, L. Wang, Z. Zhou, Z. Peng, *J. Mater. Chem. A* **2018**, *6*, 18782.

[32] X. Duan, J. Xu, Z. Wei, J. Ma, S. Guo, S. Wang, H. Liu, S. Dou, *Adv. Mater.* **2017**, *29*, 1701784.

[33] C. Jia, K. Dastafkan, W. Ren, W. Yang, C. Zhao, *Sustain. Energy Fuels* **2019**, *3*, 2890.

[34] A. C. Pérez-Sequera, M. A. Díaz-Pérez, J. C. Serrano-Ruiz, *Catalysts* **2020**, *10*, 1179.

[35] O. A. Baturina, Q. Lu, M. A. Padilla, L. Xin, W. Li, A. Serov, K. Artyushkova, P. Atanassov, F. Xu, A. Epshteyn, T. Brintlinger, M. Schuette, G. E. Collins, *ACS Catal.* **2014**, *4*, 3682.

[36] S. Nitopi, E. Bertheussen, S. B. Scott, X. Liu, A. K. Engstfeld, S. Horch, B. Seger, I. E. L. Stephens, K. Chan, C. Hahn, J. K. Nørskov, T. F. Jaramillo, I. Chorkendorff, *Chem. Rev.* **2019**, *119*, 7610.

[37] Y. Hori, K. Kikuchi, S. Suzuki, *Chem. Lett.* **1985**, *14*, 1695.

[38] Y. Hori, In *Modern Aspects of Electrochemistry*, Springer New York, New York, NY, **2008**, pp. 89–189.

[39] D. Chi, H. Yang, Y. Du, T. Lv, G. Sui, H. Wang, J. Lu, *RSC Adv.* **2014**, *4*, 37329.

[40] C. Genovese, C. Ampelli, S. Perathoner, G. Centi, *Green Chem.* **2017**, *19*, 2406.

[41] B. C. Marepally, C. Ampelli, C. Genovese, F. Tavella, L. Veyre, E. A. Quadrelli, S. Perathoner, G. Centi, *J. CO_2 Util.* **2017**, *21*, 534.

[42] A. de Lucas-Consuegra, J. Serrano-Ruiz, N. Gutiérrez-Guerra, J. Valverde, *Catalysts* **2018**, *8*, 340.

[43] S. C. Perry, P. Leung, L. Wang, C. Ponce de León, *Curr. Opin. Electrochem.* **2020**, *20*, 88.

[44] D. Kim, S. Lee, J. D. Ocon, B. Jeong, J. K. Lee, J. Lee, *Phys. Chem. Chem. Phys.* **2015**, *17*, 824.

[45] H. Xiao, W. A. Goddard, T. Cheng, Y. Liu, *Proc. Natl. Acad. Sci.* **2017**, *114*, 6685.

[46] R. M. Arán-Ais, F. Scholten, S. Kunze, R. Rizo, B. Roldan Cuenya, *Nat. Energy* **2020**, *5*, 317.

[47] R. M. Arán-Ais, R. Rizo, P. Grosse, G. Algara-Siller, K. Dembélé, M. Plodinec, T. Lunkenbein, S. W. Chee, B. R. Cuenya, *Nat. Commun.* **2020**, *11*, 3489.

[48] D. Xu, K. Li, B. Jia, W. Sun, W. Zhang, X. Liu, T. Ma, *Carbon Energy* **2022**.

[49] A. S. Varela, W. Ju, T. Reier, P. Strasser, *ACS Catal.* **2016**, *6*, 2136.

[50] J. F. de Brito, C. Genovese, F. Tavella, C. Ampelli, M. V. Boldrin Zanoni, G. Centi, S. Perathoner, *ChemSusChem* **2019**, *12*, 4274.

[51] H. Manyar, G. . Deshmukh, *Intech Open* **2020**, 281.

[52] J. H. Jones, *Platin. Met. Rev.* **2000**, *44*, 94.

[53] A. Senocrate, C. Battaglia, *J. Energy Storage* **2021**, *36*, 102373.

[54] J. Durst, A. Rudnev, A. Dutta, Y. Fu, J. Herranz, V. Kaliginedi, A. Kuzume, A. A. Permyakova, Y. Paratcha, P. Broekmann, T. J. Schmidt, *Chimia (Aarau).* **2015**, *69*, 769.

[55] S. C. Perry, S. M. Gateman, R. Malpass-Evans, N. McKeown, M. Wegener, P. Nazarovs, J. Mauzeroll, L. Wang, C. Ponce de León, *Chemosphere* **2020**, *248*, 125993.

[56] F. Marken, E. Madrid, Y. Zhao, M. Carta, N. B. McKeown, *ChemElectroChem* **2019**, *6*, 4332.

[57] X. Tan, C. Yu, C. Zhao, H. Huang, X. Yao, X. Han, W. Guo, S. Cui, H. Huang, J. Qiu, *ACS Appl. Mater. Interfaces* **2019**, *11*, 9904.

[58] B. C. Marepally, C. Ampelli, C. Genovese, T. Saboo, S. Perathoner, F. M. Wisser, L. Veyre, J. Canivet, E. A. Quadrelli, G. Centi, *ChemSusChem* **2017**, *10*, 4442.

[59] F. Cavani, F. Trifirò, A. Vaccari, *Catal. Today* **1991**, *11*, 173.

[60] C. Forano, T. Hibino, F. Leroux, C. Taviot-Guého, *Dev. Clay Sci. Vol. 1* **2006**, *1*, 1021.

[61] D. Tonelli, I. Gualandi, E. Musella, E. Scavetta, *Nanomaterials* **2021**, *11*, 725.

[62] F. Basile, L. Basini, G. Fornasari, M. Gazzano, F. Trifirò, A. Vaccari, In *Preparation of Catalysts VII*, **1998**, pp. 31–40.

[63] M. Monti, P. Benito, F. Basile, G. Fornasari, M. Gazzano, E. Scavetta, D. Tonelli, A. Vaccari, *Electrochim. Acta* **2013**, *108*, 596.

[64] T. Tabanelli, S. Cocchi, B. Gumina, L. Izzo, M. Mella, S. Passeri, F. Cavani, C. Lucarelli, J. Schütz, W. Bonrath, T. Netscher, *Appl. Catal. A Gen.* **2018**, *552*, 86.

[65] J. De Maron, M. Eberle, F. Cavani, F. Basile, N. Dimitratos, P. J. Maireles-Torres, E. Rodriguez-Castellón, T. Tabanelli, *ACS Sustain. Chem. Eng.* **2021**, *9*, 1790.

[66] A. Fasolini, D. Cespi, T. Tabanelli, R. Cucciniello, F. Cavani, *Catalysts* **2019**, *9*, 722.

[67] Fasolini, Cucciniello, Paone, Mauriello, Tabanelli, *Catalysts* **2019**, *9*, 917.

[68] L. Mohapatra, K. Parida, *J. Mater. Chem. A* **2016**, *4*, 10744.

[69] M. Khalil, J. Gunlazuardi, T. A. Ivandini, A. Umar, *Renew. Sustain. Energy Rev.* **2019**, *113*, 109246.

[70] A. Fasolini, N. Sangiorgi, E. Tosi Brandi, A. Sangiorgi, F. Mariani, E. Scavetta, A. Sanson, F. Basile, *Appl. Clay Sci.* **2021**, *212*, 106219.

[71] Y. Vlamidis, E. Scavetta, M. Gazzano, D. Tonelli, *Electrochim. Acta* **2016**, *188*, 653.

[72] F. Dionigi, Z. Zeng, I. Sinev, T. Merzdorf, S. Deshpande, M. B. Lopez, S. Kunze, I. Zegkinoglou, H. Sarodnik, D. Fan, A. Bergmann, J. Drnec, J. F. de Araujo, M. Gliech, D. Teschner, J. Zhu, W.-X. Li, J. Greeley, B. R. Cuenya, P. Strasser, *Nat. Commun.* **2020**, *11*, 2522.

[73] B. Ballarin, R. Seeber, D. Tonelli, A. Vaccari, *J. Electroanal. Chem.* **1999**, *463*, 123.

[74] E. Scavetta, D. Tonelli, *Electroanalysis* **2005**, *17*, 363.

[75] I. Gualandi, M. Tessarolo, F. Mariani, D. Arcangeli, L. Possanzini, D. Tonelli, B. Fraboni, E. Scavetta, *Sensors* **2020**, *20*, 3453.

[76] J. Choy, S. Choi, J. Oh, T. Park, *Appl. Clay Sci.* **2007**, *36*, 122.

[77] F. Millange, R. I. Walton, L. Lei, D. O'Hare, *Chem. Mater.* **2000**, *12*, 1990.

[78] A. Fasolini, S. Abate, D. Barbera, G. Centi, F. Basile, *Appl. Catal. A Gen.* **2019**, *581*, 91.

[79] K. Y. Kim, J. H. Lee, H. Lee, W. Y. Noh, E. H. Kim, E. C. Ra, S. K. Kim, K. An, J. S. Lee, *ACS Catal.* **2021**, *11*, 11091.

[80] N. Dewangan, W. M. Hui, S. Jayaprakash, A.-R. Bawah, A. J. Poerjoto, T. Jie, A. Jangam, K. Hidajat, S. Kawi, *Catal. Today* **2020**, *356*, 490.

[81] M. M.-J. Li, C. Chen, T. Ayvalı, H. Suo, J. Zheng, I. F. Teixeira, L. Ye, H. Zou, D. O'Hare, S. C. E. Tsang, *ACS Catal.* **2018**, *8*, 4390.

[82] L. Li, J. Yang, L. Li, Y. Huang, J. Zhao, *Electrochim. Acta* **2022**, *402*, 139523.

[83] K. Iwase, T. Hirano, I. Honma, *ChemSusChem* **2022**, *15*.

[84] J. Schröder, V. A. Mints, A. Bornet, E. Berner, M. Fathi Tovini, J. Quinson, G. K. H. Wiberg, F. Bizzotto, H. A. El-Sayed, M. Arenz, *JACS Au* **2021**, *1*, 247.

[85] E. Scavetta, D. Tonelli, F. Basile, F. Mariani, A. Fasolini, M. Serafini, Italian Patent Application n° 102022000025860: *"Rivestimenti catalitici a base di idrossidi doppi a strato contenenti: Cu, Mg e Al, ottenibili per via elettrochimica, per impieghi quali la riduzione elettrochimica dell'anidride carbonica",* filed on December 16th, **2022**.

[86] Q. Zhu, X. Sun, D. Yang, J. Ma, X. Kang, L. Zheng, J. Zhang, Z. Wu, B. Han, *Nat. Commun.* **2019**, *10*, 3851.

[87] S. Dongare, N. Singh, H. Bhunia, *Appl. Surf. Sci.* **2021**, *537*, 148020.

[88] I. Gualandi, Y. Vlamidis, L. Mazzei, E. Musella, M. Giorgetti, M. Christian, V. Morandi, E. Scavetta, D. Tonelli, *ACS Appl. Nano Mater.* **2019**, *2*, 143.

[89] F. Caballero-Briones, J. M. Artés, I. Díez-Pérez, P. Gorostiza, F. Sanz, *J. Phys. Chem. C* **2009**, *113*, 1028.

[90] C. Coetzee, M. Tadie, C. Dorfling, *Hydrometallurgy* **2020**, *195*, 105407.

[91] B. R. Gevers, S. Naseem, A. Leuteritz, F. J. W. J. Labuschagné, *RSC Adv.* **2019**, *9*, 28262.

[92] E. Musella, I. Gualandi, E. Scavetta, M. Gazzano, A. Rivalta, E. Venuti, M. Christian, V. Morandi, D. Tonelli, *Chem. – A Eur. J.* **2019**, *25*, 16301.

[93] R. Amini, K. Asadpour-Zeynali, *Electroanalysis* **2020**, *32*, 1160.

[94] Y. Huang, Y. Han, J. Sun, Y. Zhang, L. Han, *Mater. Today Chem.* **2022**, *24*, 100895.

[95] E. Musella, I. Gualandi, M. Giorgetti, E. Scavetta, F. Basile, A. Rivalta, E. Venuti, F. Corticelli, M. Christian, V. Morandi, D. Tonelli, *Appl. Clay Sci.* **2021**, *202*, 105949.

[96] D. Cosano, D. Esquivel, F. J. Romero-Salguero, C. Jiménez-Sanchidrián, J. R. Ruiz, *Colloids Surfaces A Physicochem. Eng. Asp.* **2020**, *602*, 125066.

[97] J. Liu, Y. Tian, Y. Chen, J. Liang, L. Zhang, H. Fong, *Mater. Chem. Phys.* **2010**, *122*, 548.

[98] E. Scavetta, A. Mignani, D. Prandstraller, D. Tonelli, *Chem. Mater.* **2007**, *19*, 4523.

[99] F. Basile, P. Benito, G. Fornasari, M. Monti, E. Scavetta, D. Tonelli, A. Vaccari, *Catal. Today* **2010**, *157*, 183.

[100] H. P. Klug, L. E. Alexander, *2nd Ed. John Wiley Sons* **1974**, 618.

[101] S. Miyata, *Clays Clay Miner.* **1983**, *31*, 305.

[102] S. Marappa, S. Radha, P. V. Kamath, *Eur. J. Inorg. Chem.* **2013**, *2013*, 2122.

[103] F. P. Lohmann-Richters, B. Abel, Á. Varga, *J. Mater. Chem. A* **2018**, *6*, 2700.

[104] M. C. O. Monteiro, F. Dattila, B. Hagedoorn, R. García-Muelas, N. López, M. T. M. Koper, *Nat. Catal.* **2021**, *4*, 654.

[105] S. Lu, Y. Wang, H. Xiang, H. Lei, B. Bin Xu, L. Xing, E. H. Yu, T. X. Liu, *J. Energy Storage* **2022**, *52*, 104764.

[106] M. Jia, Y. Zhang, Y. Bao, J. Wang, A. Xu, *Green Chem. Lett. Rev.* **2018**, *11*, 230.

[107] N. E. H. Hadj-Abdelkader, A.-P. Beltrao-Nunes, F. Belkhadem, N. Benselka, R. Roy, A. Azzouz, *Appl. Clay Sci.* **2020**, *198*, 105829.

[108] S. Ishihara, P. Sahoo, K. Deguchi, S. Ohki, M. Tansho, T. Shimizu, J. Labuta, J. P. Hill, K. Ariga, K. Watanabe, Y. Yamauchi, S. Suehara, N. Iyi, *J. Am. Chem. Soc.* **2013**, *135*, 18040.

[109] E. D. Goodman, J. A. Schwalbe, M. Cargnello, *ACS Catal.* **2017**, *7*, 7156.

[110] L. Wu, K. E. Kolmeijer, Y. Zhang, H. An, S. Arnouts, S. Bals, T. Altantzis, J. P. Hofmann, M. Costa Figueiredo, E. J. M. Hensen, B. M. Weckhuysen, W. van der Stam, *Nanoscale* **2021**, *13*, 4835.

[111] C. C. L. McCrory, S. Jung, I. M. Ferrer, S. M. Chatman, J. C. Peters, T. F. Jaramillo, *J. Am. Chem. Soc.* **2015**, *137*, 4347.

TABLE OF CONTENT

M. Serafini, F. Mariani, A. Fasolini, E. Tosi Brandi, E. Scavetta, F. Basile*, and D. Tonelli*

Electrosynthesized CuMgAl Layered Double Hydroxides as New Catalysts for the Electrochemical Reduction of CO_2

New CuMgAl Layered Double Hydroxides are obtained by a one-step electrodeposition over a carbonaceous gas diffusion membrane and are characterized by an intimate contact with Cu^0/Cu^+ species. The optimized nanostructured material shows unprecedented electrocatalytic activity toward the CO_2 conversion to CH_3COOH (2.0 mmol g_{cat}^{-1} h^{-1} productivity and 100% selectivity) at low cathodic potential (-0.4 V vs RHE).